Chapter 1

Introduction

The atomic nucleus is a unique quantum system, consisting of protons and neutrons. A strong force binds these nucleons. One of the nucleus's most intriguing and fundamental emergent properties is the shape that these nucleons are distributed across. Understanding the various properties through the many-body nucleonic interactions in the nucleus motivates us to study nuclear physics. Other than this, it is also necessary to reveal how these nucleons are distributed across the nucleus. A few nuclei have spherical shapes in their ground states, but at high spin, they show different shapes in the same nucleus. It is interesting to investigate the nuclear shape transitions at high angular momentum, as this continues to be one of the more demanding aspects of excited nuclei. Deformed nuclei can schematically be classified as prolate, oblate and triaxially deformed (see Fig. 1.1). This classification depends on the value of β (quadrupole deformation parameter), $\beta > 0$ corresponds to prolate, $\beta = 0$ to spherical, and $\beta < 0$ to oblate deformation. The choice of variation of shape parameter extends from $\gamma = 0$ to 2π. Another parameter which is most often used to describe the axial deformation is ε_2, which can be associated with β such that $\varepsilon_2 \approx 0.95\beta$.

Variation of $\gamma = 0^\circ \rightarrow +60^\circ$ represents the rotation of nucleus around the shortest principal axis, $\gamma = 0^\circ \rightarrow$ -60° represent the rotation of nucleus around the intermediate

axis and = -60° → -120° represent rotation around the longest principal axis see Fig. 1.1. The parameters β and γ are the axial and triaxiality deformation parameters. The figure is taken from [2]. The nucleus becomes more stable if the number of nucleons (protons and neutrons) Z or N is equal to 2, 8, 20, 28, 50, 82 and 126. These numbers are called magic numbers [3]. The existence of a magic number is explained using the shell model, and it also describes the spin and parities of low low-lying states of closed major shell nuclei [4]. Various shapes can also coexist at the same excitation energy and spin in a given nucleus.

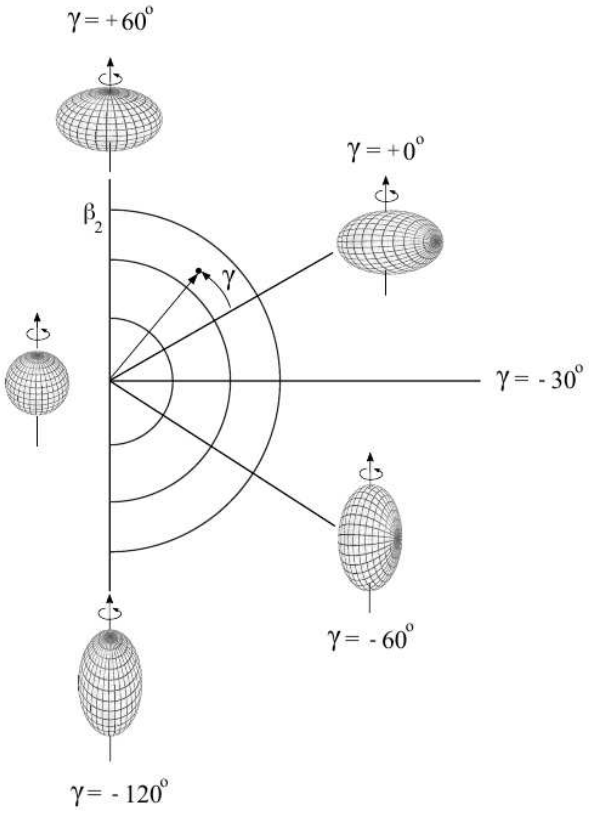

Figure 1.1 Schematic diagram of the shape parameters in rotating quadrupole deformed nuclei [2]

.

In order to describe the nuclear shape at high spin, a variety of theoretical models have been proposed. Experimental information is needed in order to test the validity of and/or improve the model descriptions in different regions of the nuclear chart. One important

tool for studying nuclear properties is gamma-ray spectroscopy. Two main features present in nuclear structure, these being single-particle effect (described within the framework of the shell model) and collective effects (described with the cranked Nilsson Model). The single-particle effect is dominant in near-spherical nuclei, occurring in the presence of a strong spin-orbit interaction, whereas collective effects are expected to dominate in deformed nuclei.

The study of nuclei in the A≈90 region is an excellent area to investigate the impact of Z = 38,40 subshell closure and N = 50 shell closure on the level structures. Many studies have been performed in this area, leading to a deep understanding of nuclear physics.

The level structures for Sr, Y, Zr, Nb, Mo, Tc, Ru, and Rh nuclei have been thoroughly described within the shell model framework, as shown by references [5–12]. The low-lying levels of such nuclei can be understood in the $\pi(p_{1/2}, g_{9/2})$ configuration space whereas the high-spin states in these nuclei can be studied as an outcome of the $\pi(p_{3/2}, f_{5/2}, p_{1/2}) \rightarrow g_{9/2}$ proton excitations and $\nu(g_{9/2} \rightarrow (d_{5/2}, g_{7/2})$ neutron excitations across the N = 50 magic shell gap. The $A \approx 90$ mass region becomes quite interesting for determining the effective proton-neutron residual interaction.

^{92}Nb, being an odd-odd nucleus, becomes quite instrumental for determining the effective proton-neutron residual interaction. The nucleus has one lone proton and one lone neutron above the Z = 40 subshell closure and N = 50 magic core. The contribution of these valence nucleons coupled with core excitations may lead to the understanding of mechanisms responsible for the generation of high-spin states in this mass region. This coupling mechanism plays a crucial role in the dynamics of nuclear structure and is an area of great interest within the field of nuclear physics. Therefore, excited states of these nuclei have attracted a lot of attention in theoretical and experimental works. The study of odd-odd nuclei is less extended since the level structure of odd-odd nuclei is complicated due to a high level of density. Exploring odd-odd nuclei provides a crucial understanding

of valence particle interactions and the significant impact of specific proton and neutron orbitals on nuclear shape.

This thesis aims to understand how nearly closed shell nuclei in the mass $A \approx 90$ regions generate angular momentum. At lower energies, these nuclei display irregular excitation(single-particle excitation), while band-like structures(collective rotation) have been observed in the higher excitation energy domain [5–12]. One of the common characteristics of these bands is enhanced $M1$ strengths with very weak or completely suppressed $E2$ crossovers. One of the examples is shown in Fig. 1.2.

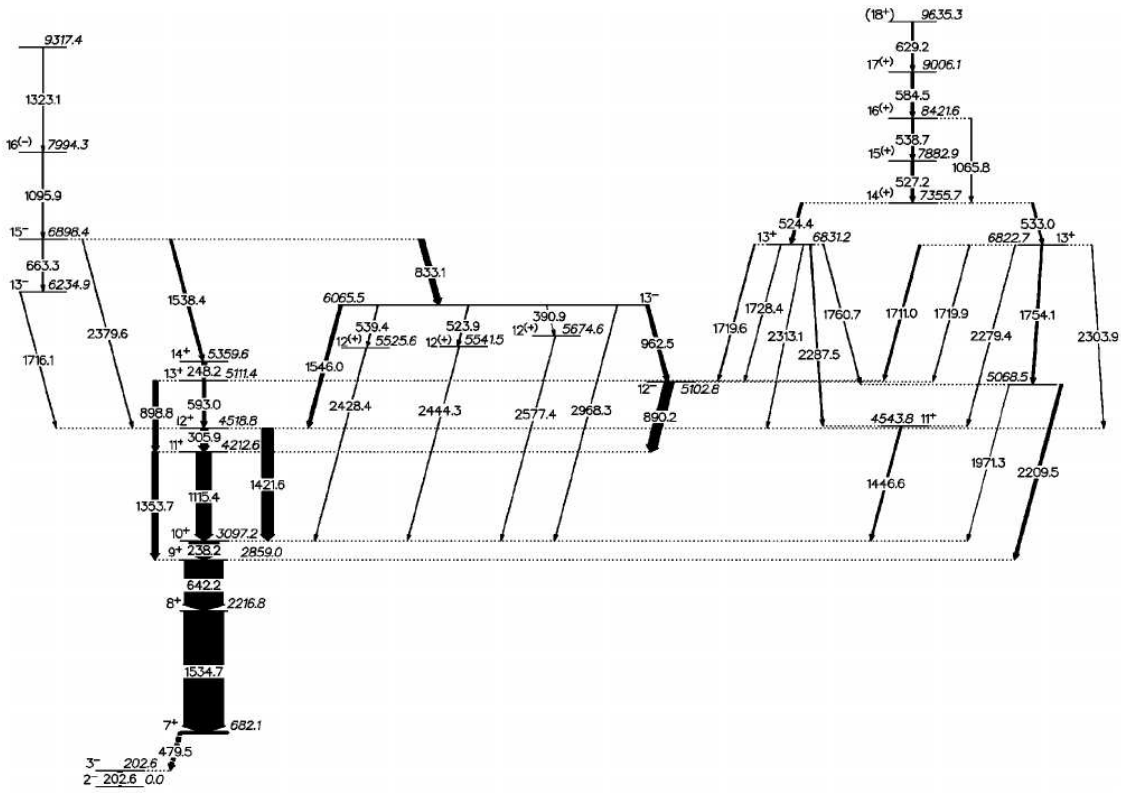

Figure 1.2 Examples of angular momentum generation through single-particle excitations at lower excitation energy and through collective excitations at higher excitation energy in nearly-spherical ^{90}Y. This is the near yrast level scheme for ^{90}Y, reproduced from reference [6].

1.1 Single-particle excitation:

Spherical or near-spherical nuclei that generate angular momentum by rearranging their valence nucleons exist near the closed shells. In Figure 1.2, the lower part of a level scheme of ^{90}Y is an example of such type of excitation is shown. The total angular momentum is generated due to the sum of the individual angular momentum of valence nucleons that are not coupled to spin-zero. The core makes no contribution to the angular momentum generation for the low-spin part; however, as the angular momentum contribution of valence nucleons gets consumed and further spins are generated, then core-excitation has to be included.

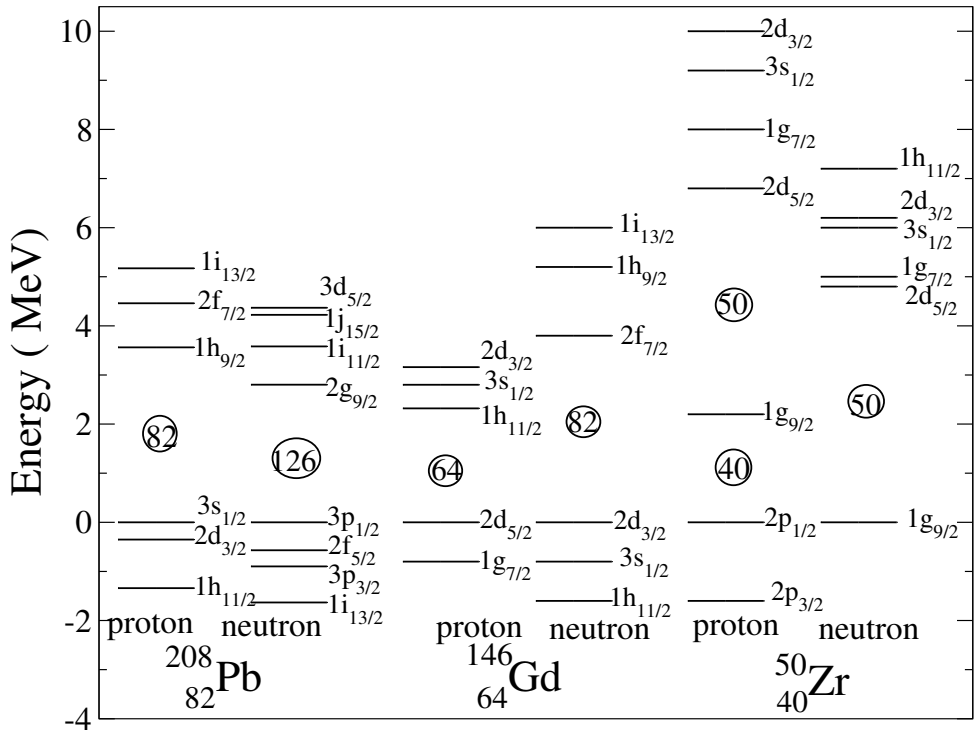

Figure 1.3 Single-particle levels in the ^{208}Pb, ^{146}Gd region and in the ^{90}Zr region. The single-particle energies are given with respect to an arbitrary zero point.

1.2 Mass Region $A \approx 90$

The nucleus in the mass $A \approx 90$ region exhibits similarity with $A \approx 150$, ≈ 210 region in terms of shell gaps. A schematic diagram showing the similarity in valence space for all three mass regions is shown in Fig. 1.3.

1.3 Isomeric states

The excited states have significantly longer half-lives than the typical excited states of nuclei. The hindrance posed to isomeric decay is mostly due to three reasons: different structural matrix elements of the initial and final states, small decay energy, and the large change in angular momentum. On the basis of hindrance mechanisms to their respective decays, the isomers can be classified into spin and seniority isomers in spherical regions. On the other hand, isomers are categorized as shape, K and fission isomers in deformed regions, where K is the total angular momentum projection on the axis of symmetry for axially deformed nuclei [13–16]. The existence of different orders of a lifetime in an isomeric state invokes the implementation of different physical and instrumental treatments in various applications. A large number of isomers de-exciting via enhanced $M2/E3$ transitions have been identified in near-spherical Bi-At-Rn-Fr nuclei [17–22] in the mass 210 region and Tb-Ho nuclei [23, 24] in mass 150 regions. The lifetime of these isomers varies from a few nanoseconds to microseconds. The existence of such isomers may help us obtain a detailed understanding of nuclei near the doubly magic shell closure because such states provide quite pure shell-model configurations in the low-lying levels of the neighboring nuclei. In addition, multiplets of states formed by weak coupling of the single-particle configurations with the collective states in the neighboring magic nuclei can further help us in understanding the competition between single-particle and collective phenomenon [25, 26]. Copenhagen group has highlighted that one of the most sensitive

ways of testing the particle vibration coupling by observing the effects of small admixtures of single-particle levels in the states of weakly coupled multiplets and vice versa [27, 28]. In order to analyze the existence of the same kind of isomers in different mass regions, we tally the fermi orbitals in mass 210, 150 and mass 90 regions (see Fig. 1.3). The existence of Fermi space around the magic shell closure in all three above-mentioned mass regions involves excitation of either type of nucleons across low-j orbitals and high-j intruder orbitals.

The empirical shell model has provided a particularly good interpretation of states in nuclei in the trans-lead region, see for example [29] and references therein. One key to the successful application to complex nuclei, especially in the $A \approx 210$, is the availability of comprehensive information derived from simple systems near the doubly closed ^{208}Pb core. Although empirical energies are relatively easy to derive, other properties, such as electrical quadrupole moments, are less tractable. The ^{210}Po and ^{211}At were observed to be the first nuclei to have states where the $\pi i_{13/2}$ quadrupole moment was accessible, though the quadrupole moment for the $\pi i_{13/2}$ orbital was extracted indirectly [30]. Isomers based on $M2/E3$ transitions in ^{209}Bi provide information on proton $3s_{1/2} \rightarrow 2f_{7/2}$ pure $E3$ and proton $1i_{13/2} \rightarrow 1h_{9/2}$ or neutron $1j_{15/2} \rightarrow 1h_{11/2}$ pure $M2$ character [17]. With motivations stated above, the lion's share of work was done in $A \approx 200$ region. These observations and similarities in Fermi space (see Fig. 1.3) prompted the nuclear structure community to extend such studies in $A \approx 150$. In this mass region, the nuclei ^{147}Tb (N=82, Z=65) and ^{148}Tb (N=83, Z=65) have been studied by R. Broda *et al.* [24]. , who reported uncommon low-lying isomers based on $M2/E3$ transitions in the given nuclei. Similar to ^{209}Bi (Z = 83), the observed isomers de-excite to the ground states of the respective nuclei. It is evident from the comparison of $E3$ enhancement factors (31 and 28 W. u. for ^{147,148}Tb respectively) that the $15/2^+$ and 11^- isomers in ^{147,148}Tb respectively and the $13/2^+$ isomer ($E3$ strength $\approx$ 44 W.u.) at 997 keV in ^{147}Gd involve the coupling of the

valence nucleon(s) to the 3^- octupole excitation of the ^{146}Gd core nucleus. Hamamoto [27] has considered the problem of the coupling of a single particle (or hole) to the octupole vibration and has presented the four lowest-order Feynman diagrams which contribute to the energy shifts in a particle plus phonon multiplet. It is expected that the composition of the collective octupole excitation in terms of shell model wave functions is reflected in its behavior when coupling to those orbitals. Knowledge of the composition of this phonon is of interest and has been helpful in understanding the effect of the Pauli principle on particle-phonon coupling. The influence of the Pauli principle rather depends upon whether the particles in a particle-phonon coupled state arrange themselves symmetrically or antisymmetrically. Authors have stressed onto the need for further experimental data on coupled states as the large-scale shell model calculations are able to describe the collective octupole states around ^{208}Pb [31, 32] whereas the energies of the octupole states could not be reproduced accurately. The above review of isomers based on $M2/E3$ transitions in $A \approx 210$ and 150 highlights the effect of valence space around the magic closure and the existence of isomeric states dominated by particle-phonon coupling. As evident from Fig. 1.3, the Fermi region around a doubly magic core in $A \approx 90$ resembles that of the higher mass region counterparts.

Isomers are common in the mass 90 regions (either low- or high-spin isomers). Especially, the long and short-lived isomers have been systematically observed at low and higher spin states in odd mass nuclei of $A \approx 90$ regions, see Fig.1.4. The nuclei in the vicinity of the semi-magic core ($^{90}_{40}$Zr) are predominantly dependent on shell-model excitation. In isotones with $N = 50$, many levels beyond Z=38 can be described in first order by proton configurations with $1g_{9/2}$, and $2p_{1/2}$ orbitals. The nuclei with $N = 51$ are similarly described by the coupling of a $2d_{5/2}$ neutron-particle orbital to corresponding $N = 50$ configurations.

There are multiple motivations for studying the properties of low-spin isomers in this region. The isomers are interesting in themselves as a means for testing the theoretical calculations that predict their existence on the basis of a model assuming "rotation" along a symmetry axis of an oblate nucleus [33] or as a result of the coupling of several valence nucleons above the closed shell [17–24].

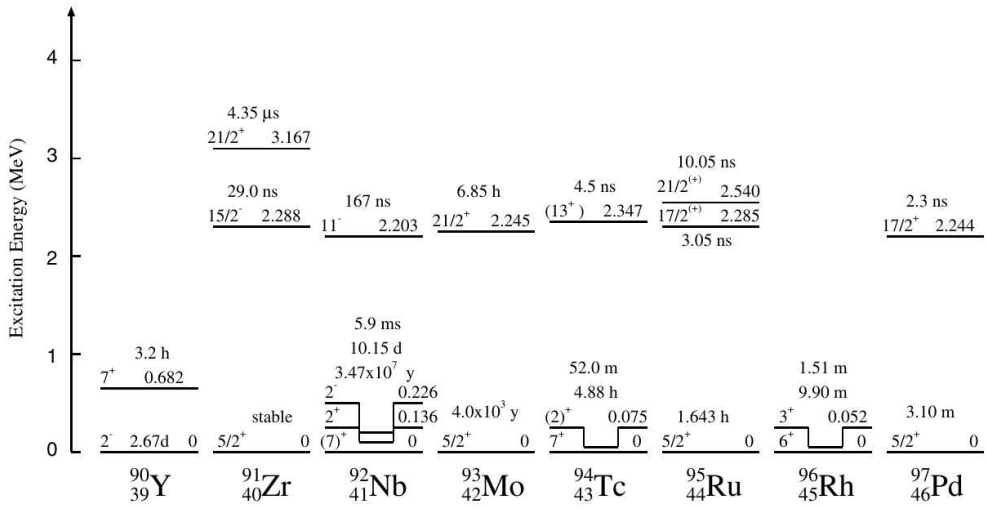

Figure 1.4 Experimental systematics of isomers in $N = 51$ isotones [11].

In addition, in the contemporary research field of nuclear astrophysics, the isomers find a great role to play in. Specially such isomers are known as astromers. Despite the experimental and theoretical progress in terrestrial studies, uncertain regarding the population of nuclear isomers in astrophysical environments still remains a mystery. Astrophysical nucleosynthesis calculations are mostly based on accurate nuclear reaction rate inputs. Either only the ground-state rate is used, or the levels are considered to be in a thermal-equilibrium probability distribution. The presence of an isomeric state can disrupt the accuracy of both approaches. While decaying to a lower excited state, a nucleus can get caught in an isomeric trap before it reaches the ground state. This may lead to a situation where the nucleus will not necessarily undergo subsequent reactions at the ground state rate. Isomers can also cause the probability distribution of nuclear energy levels to fail to

reach thermal equilibrium [34, 34]. The example of ^{92}Nb is quite profound in this regard. The half-life of the ground state at $I = 7^+$ is of the order of 10^7 years due to hindered β decays to low-lying states of ^{92}Zr or ^{92}Mo. However, the first excited state at $I = 2^+$ does also has 10 days of half-life as direct EM transition with $M5$ or $E6$ multipolarity is not favored. Mohr has investigated the effect of the 2^+ isomeric state in the production of ^{92}Nb in any explosive scenario and did not find the isomer to be effective enough in deciding the decay rates. However, the author has not negated the possibility of isomeric contribution towards the population of ^{92}Nb at further lower temperatures ($T \approx 8$ keV) [35].

1.4 Lifetime measurement

Spherical or near-spherical nuclei exhibit spectra of single-particle excitations. On the other hand, observation of regular rotational-like sequences of a strongly enhanced magnetic dipole ($M1$) transitions in several 90 mass nucleus was therefore very surprising [6, 7, 11]. One of the common characteristics of these bands is enhanced $M1$ strengths with very weak or completely suppressed $E2$ crossovers, or were not even observed at all, in some cases. A significant observation has come from the accurate lifetime measurements of excited states in the $\Delta I = 1$ bands in this mass region [6, 7]. The experimentally deduced reduced transition probabilities $B(M1)$ are large (up to several μ_N^2) and remain constant with increasing spin see Fig. 1.5.

These features of the $M1$ bands showed that they can be understood in terms of the collective rotation of deformed nuclei.

In this thesis work, our goal is to comprehend the process behind the creation of angular momentum in slightly deformed nuclei with a mass around $A \sim 90$. These nuclei tend to display irregular excitation at lower energies, while band-like structures have been observed at higher excitation energies. The observation of the bands would provide a platform to understand the evolution of collectivity based on particle-hole excitations and

understand the observed phenomenon in the framework of the cranked Nilsson Strutinsky model calculation.

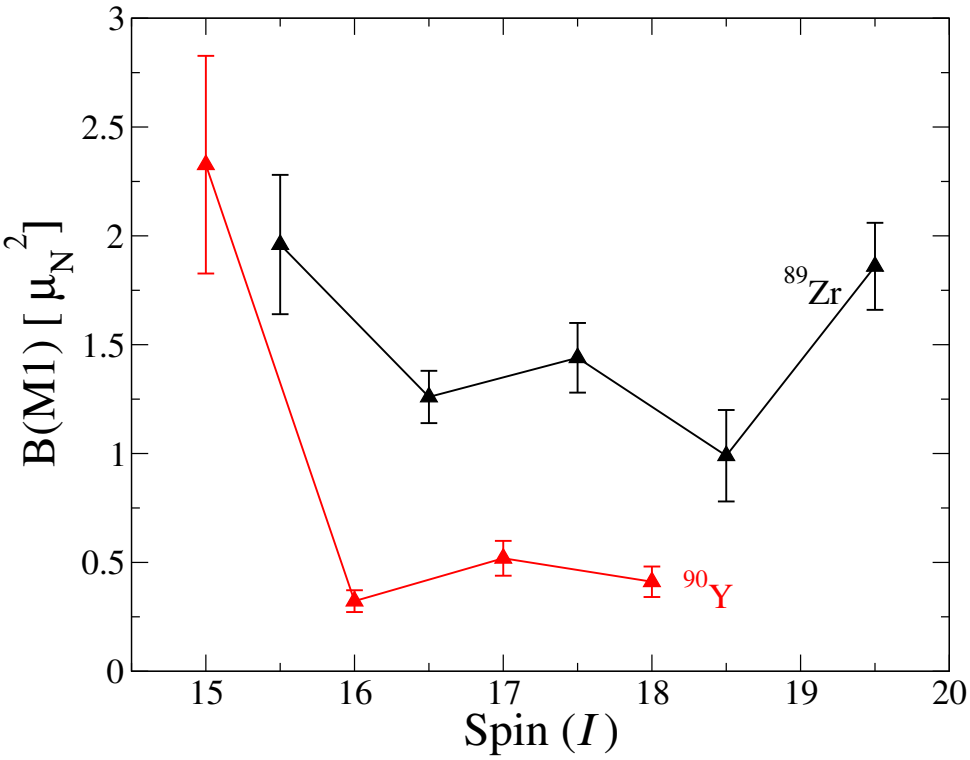

Figure 1.5 The characteristic diagram of $B(M1)$ values with spin I for the magnetic rotational bands in ^{89}Zr and ^{90}Y nuclei [6, 7].

1.4.1 Collective excitation:

The collective motion of nucleons leads to rotation and vibration which is the main mechanism behind collective nuclear excitations. For nuclei in mass 90 regions, rotational bands [6, 7, 11] are observed and their excitation energies follow the $I(I+1)$ rotational pattern, where 'I' is the total angular momentum.

The presence of collective and single-particle excitation within a nucleus also provides the motivation to carry out studies on nuclear structural properties up to a large angular momentum and excitation energy. Interestingly, nuclei tend to undergo shape changes

from prolate to non-collective oblate states at high spin. Valence nucleons in partially filled shells gradually align their angular momentum along the rotational axis for nuclei with a few particles outside the core. In quantum systems, since rotation is forbidden around the symmetry axis, the band terminates at a particular spin value. Hence, the collectivity within the nucleus is lost. The phenomenon is known as band termination [36]. Higher spin states beyond the termination might be produced by exciting particles from the core to the excited states.

The stability of spherical nuclei is determined by the presence of large shell gaps in their single-particle energy levels. These shell gaps are explained in detail in Chapter 3. Shell gaps in the single-particle energy spectrum depend on the deformation of the nucleus. In the absence of any spin-orbit coupling, shell gaps originate at certain particular values of the ratio of the principal axes in the ellipsoidal nucleus. Calculations (either with harmonic oscillator potential or with more realistic potentials [37–39]) predict various shapes with a change in deformation.

The cranked Nilsson-Strutinsky (CNS) model can explain the general features of rotating nuclei,(detailed explanation in chapter 3) where shell effects are added to the rotating liquid drop energy, see, e.g., [40], i.e., the dependence on angular momentum I is typically determined on average using the formula $I^2/(2J_{rig})$, where J_{rig} is the rigid body moment of inertia. The triaxial rotation is often observed due to the largest J_{rig} value which is linked to the rotation around the shortest principal axis. The bands approaching termination in the A = 60 and A = 110 regions [36], for the strongly deformed triaxial bands in Lu isotopes [41] and for the less deformed $^{138-140}$Nd bands [42] are some example of this kind of rotation. On the other hand, pairing correlations at low spin reduce the collective moment of inertia significantly compared to a rigid body. Furthermore, when considering pairing correlations the moment of inertia behaves similarly to the hydrodynamic moment of inertia, being

largest for rotation about the intermediate axis. Thus, at low spin rotation about this axes is energetically favored in nuclei with a triaxial ground state, see, e.g., [43].

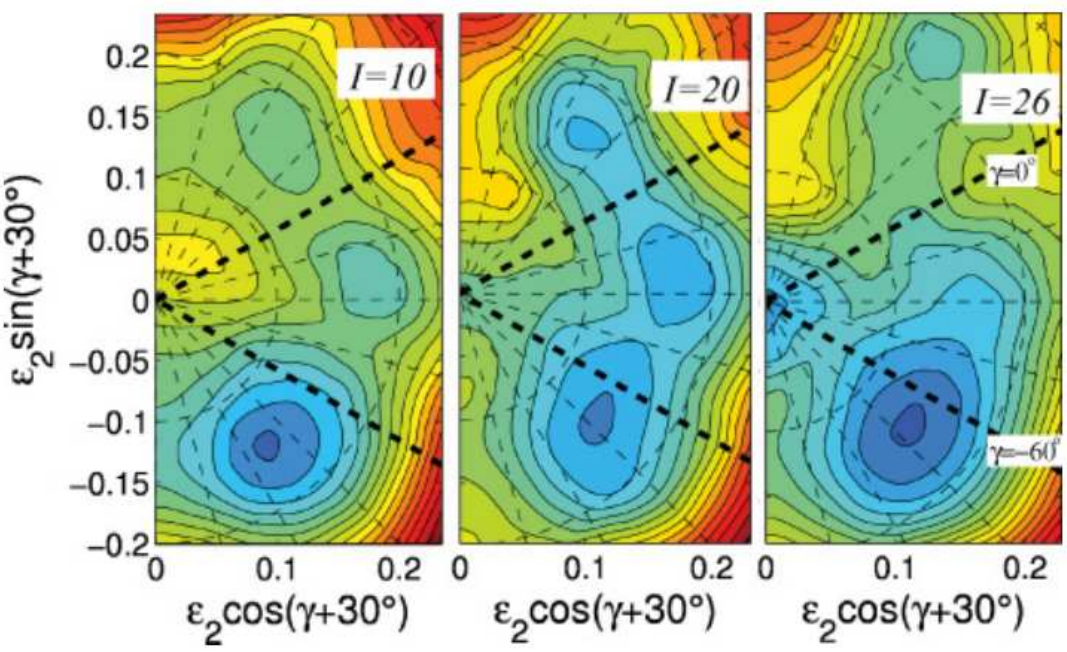

Figure 1.6 Calculated total energy surfaces with pairing included for the $(\pi, \alpha)_p$ $(\pi, \alpha)_n$ = $(+, 0)_p$ $(+, 0)_n$ combination of quantum numbers at I = 10, 20, and 26$\hbar$. At each point, the total energy has been minimized with respect to ε_4, $\lambda_{p,n}$ and $\Delta_{p,n}$ as well as quasiparticle configuration. The contour line separation is 0.25 MeV. The figure is drawn for γ = [-120°, 60°] with the γ = 0° and -60° axes labeled in the I = 26 surface in ^{142}Gd [44].

The ground state band of even-even nuclei has no aligned particles for angular momentum. However, shell effects can cause rotation around the intermediate axis in cases where pairing correlations are not significant. ^{77}Kr is an example where rotation around this axis explains a specific rotational band due to significant triaxial deformation [45]. Later, at high-spin band rotation occurred around the classically unfavored longest principal axis (the axis with the smallest J_{rig}) was observed in ^{142}Gd [44]. Within the intermediate spin range, rotation occurred around the three different minima corresponding to three different principal axes. The high-spin part of the observed $(+, 0)_1$ [44] yrast band linked to a $\pi(h_{11/2})^4\nu(h_{11/2})^{-2}$ configuration which is triaxial with $\varepsilon_2 \approx 0.15$ and γ going from -80°

to -70° as spin increases, i.e., the high-spin states in the $I \approx 26$–34 range were understood as to be built from rotation around the longest principal axis see Fig.1.6.

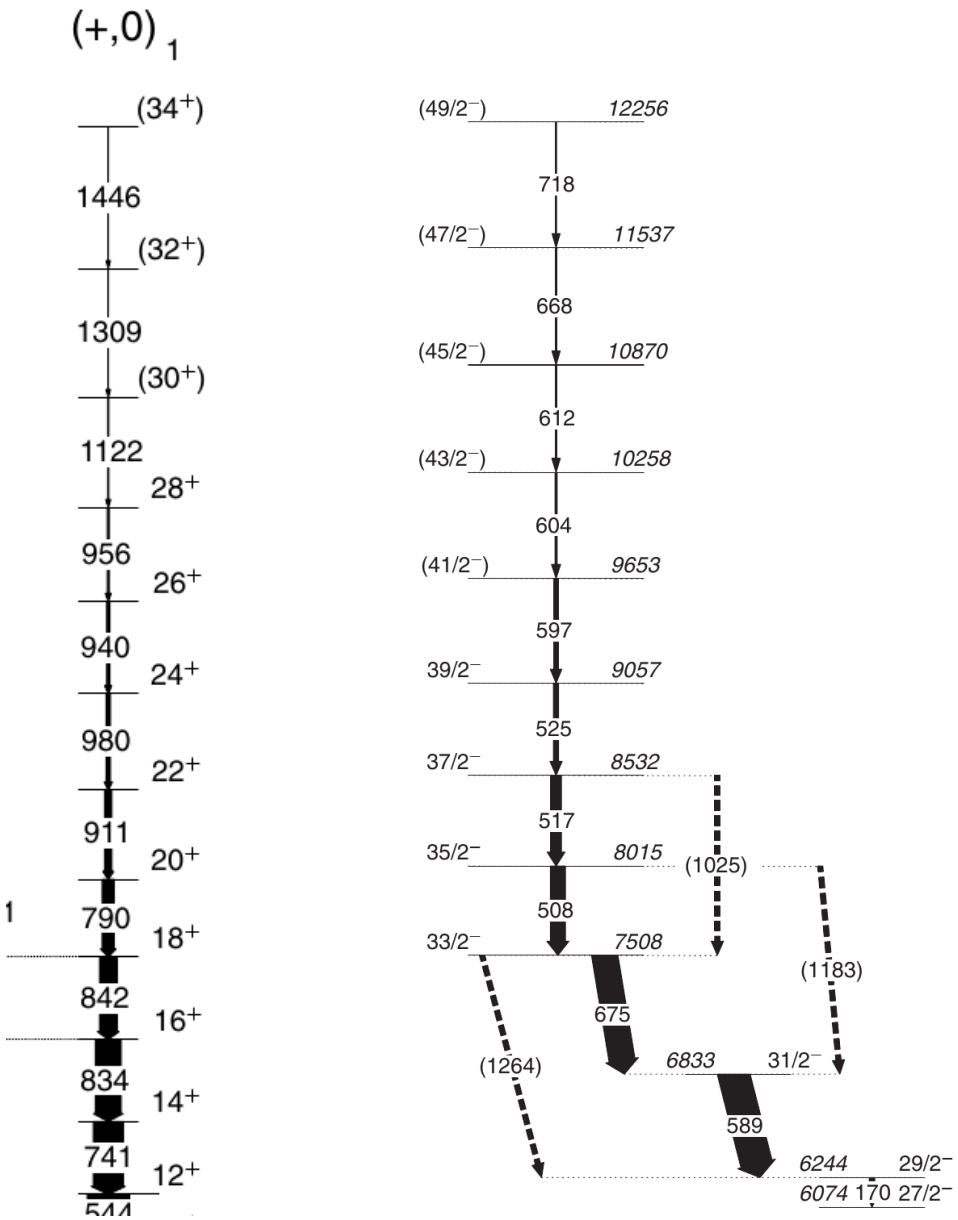

Figure 1.7 Partial (high-spin)level scheme of (a) ^{142}Gd adapted from [44] (b) ^{89}Zr adapted from [7].

Similar observations were made in ^{89}Zr ($Z = 40$, $N = 49$; $A \approx 90$) where a regular dipole band has been observed (shown in right of Fig. 1.7) by S. Saha *et al.* [7] where

the rotation around the longest principal axis shows up very clearly with γ values around -60° in Fig.1.8. In both the cases ^{89}Zr and ^{142}Gd, the nucleus rotates around the longest axis due to the distribution of neutron holes since nuclei in both the mass regions have comparable Fermi space ($\nu((ds)^{-2}h_{11/2}^{-2})$ and $\nu(g_{9/2}^{-2}(dg)^{1})$ respectively).

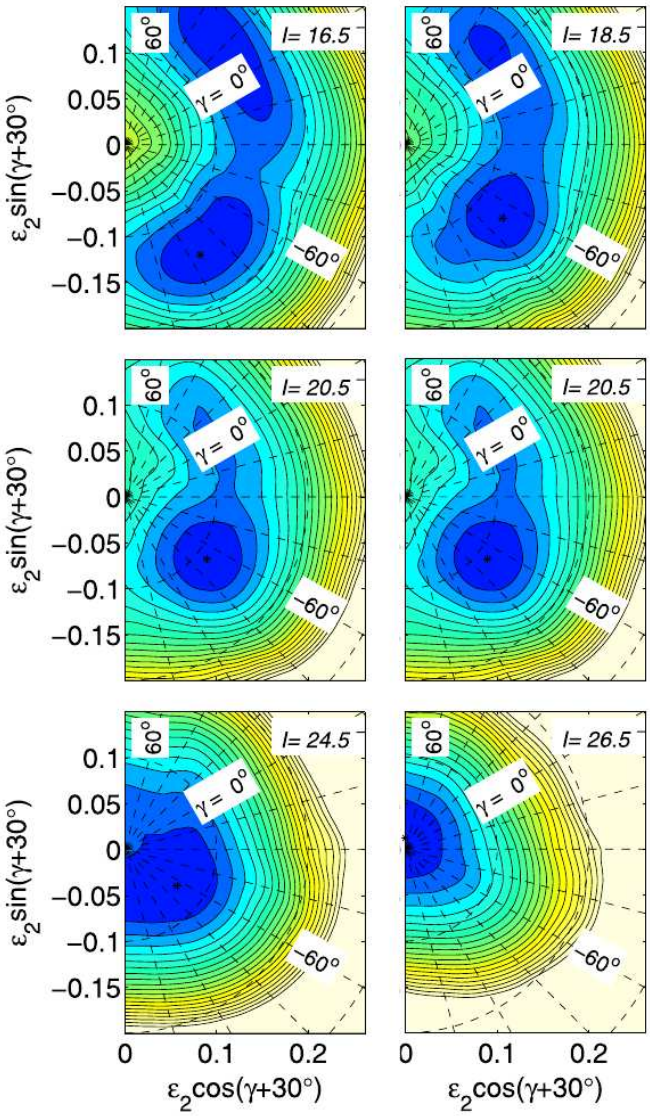

Figure 1.8 Calculated total energy surface plot for ^{89}Zr. The contour line separation is 0.25 MeV [7].

One way to understand the evolution of shape is by looking at the distribution of particles and holes in the valence orbitals. If particles align along an axis, the matter

becomes more concentrated around the equator that corresponds to that axis. On the other hand, if there is alignment of holes, the matter density in the equator decreases, which promotes rotation along the longest principal axis.

One fascinating aspect to consider is how the quantity of valence protons(holes) and neutrons(holes) impacts the transition from prolate to oblate states at high spin. It is intriguing to observe the shape changes that occur during this transition and how it affects the overall behavior of the system e.g. ^{89}Y with one proton hole($Z = 39$, $N = 50$), ^{90}Nb with one proton particle and one neutron hole($Z = 41$, $N = 49$) and ^{90}Zr with no hole/particle ($Z = 40$, $N = 50$).

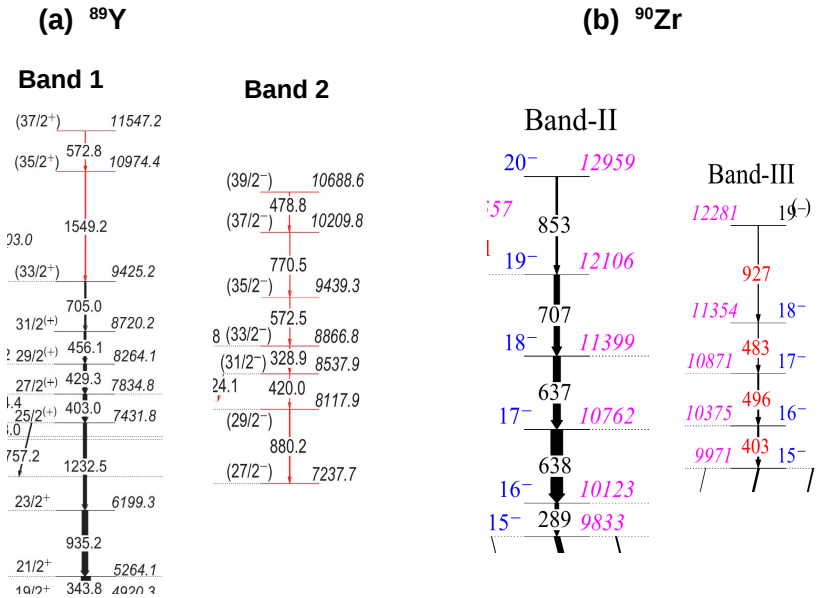

Figure 1.9 Panel (a) dipole bands of ^{89}Y and Panel (b) dipole bands of ^{90}Zr.

1.5 ^{89}Y

A couple of bands, each with positive and negative parity states respectively, were reported experimentally in ^{89}Y (see panel (a) of Fig.1.9) by Z. Q. Li *et al.* [46]. In Fig. 1.10

the calculated energies for the [43;11] ($\pi((fp)^{-4}(g_{9/2})^3 \otimes \nu(g_{9/2})^{-1}(gd)^1$) and [32;22] ($\pi((fp)^{-3}g^2_{9/2})) \otimes \nu(g^{-2}_{9/2}(gd)^2)$) configurations are compared with those of the experimentally observed bands. The top panel shows the experimental energies of positive and negative parity bands in ^{89}Y. It is to be mentioned that for clarity of calculation, the even spin states (closed symbols) of bands 1 and 2 are displayed as 1a and 2b bands, whereas the odd spin (open symbols) are shown as 1b and 2a bands. The calculated energies of the two low-energy configurations which come close to the experimental bands, [43;11] and [32;22], are displayed in the middle panel of Fig. 1.10. The even- and odd-spin states of band 1 have been compared with configurations [$43_-;1_+1_+$] and [$43_-;1_+1_-$] respectively. The energy of the [43:11] configuration is in fair agreement with the experiment in this spin range. Therefore, band 1 can be explained by the contribution from $\pi((fp)^{-4}g^3_{9/2})) \otimes \nu(g^{-1}_{9/2}(gd)^1)$. With this configuration, a total spin of 24.5 $\hbar$ can be generated.

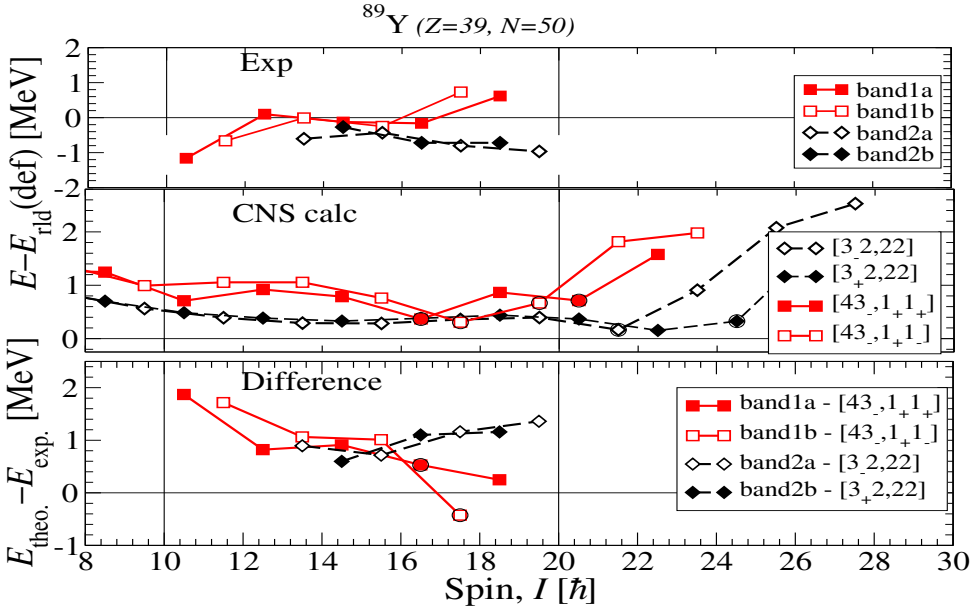

Figure 1.10 Excitation energies relative to rotating-liquid drop energy, for observed (upper panel) and calculated (lower panel) valence-space states for ^{89}Y. Difference between the observed and calculated results have been shown in the third panel.

The probable nuclear shapes for band 1 are discussed in Fig.1.11 which shows the evolution of stable nuclear shapes as a function of spin. For states up to $I = 15.5\,\hbar$ the energetically favorable minimum corresponds to negative γ values with $\gamma \approx$ -90° and $\varepsilon_2 \approx 0.15$. i.e., rotation around the longest principal axis. However, for high-spin levels, the energetically favorable configuration [43;11] $\pi((fp)^{-4}(g_{9/2})^3 \otimes \nu(g_{9/2})^{-1}(gd)^1)$ is stabilized with $\gamma \approx$ -120° and $\varepsilon_2 \approx$ -0.1, which is non-collective prolate as per the Lund convention.

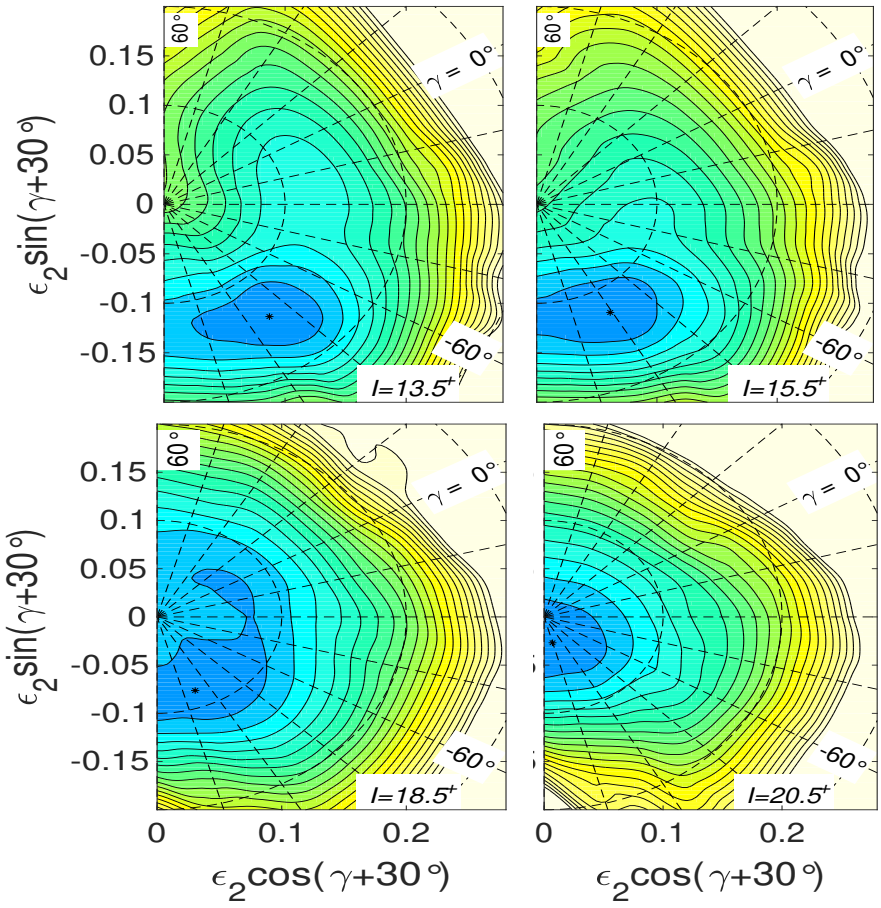

Figure 1.11 Calculated total energy surfaces plots for positive parity (band 1) spin of 13.5 $\hbar$, 15.5 $\hbar$, 18.5 $\hbar$ and 20.5 $\hbar$ for [43;11] $\pi((fp)^{-4}(g_{9/2})^3 \otimes \nu(g_{9/2})^{-1}(gd)^1)$ in ^{89}Y. The contour line separation is 0.25 MeV.

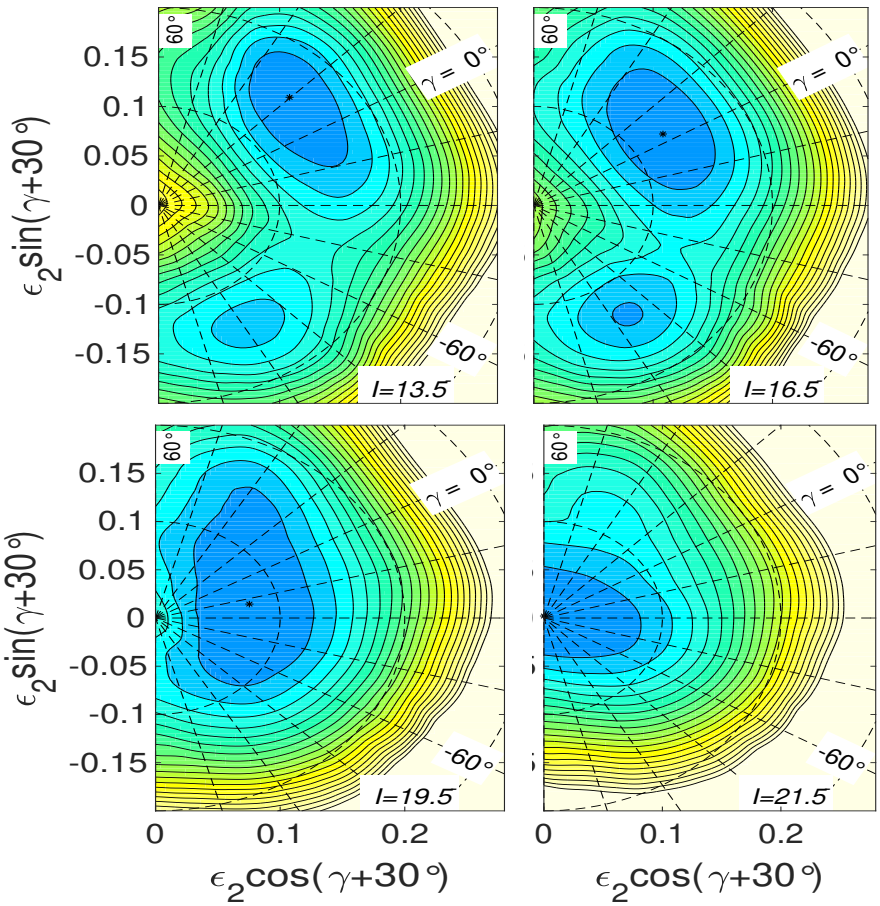

Figure 1.12 Total energy surfaces for band 2, the configuration [32;22] $\pi((fp)^{-3}g^2_{9/2}))\otimes \nu(g^{-2}_{9/2}(gd)^2)$ for spins 13.5$\hbar$ to 21.5$\hbar$ in ^{89}Y. The contour line separation is 0.25 MeV.

Further, even- and odd-spin states of the negative parity band are compared with configurations, [3$_+$2;22] and [3$_-$2;22] respectively. Band 2 agrees well with $\pi((fp)^{-3}g^2_{9/2}))\otimes \nu(g^{-2}_{9/2}(gd)^2)$ configuration over the given spin range as the difference between the two stays non-zero but stays at a constant positive value around 1 MeV (see Fig.1.10).

Potential energy surfaces for the configuration [32;22] $\pi(fp)^{-3}(g_{9/2})^2\otimes\nu(g_{9/2})^{-2}(gd)^2$ show that the configuration [32;22] is stabilized with a shape at γ values around -20° that corresponds to rotation around the intermediate principal axis at high spin. However, for spin values up to $I = 18.5\hbar$, the lowest minimum corresponds to positive γ values and $\varepsilon_2 \approx$ 0.12, i.e., rotation around the shortest principal axis (see Fig.1.12). It is noteworthy that

in the nuclei of ^{89}Zr and ^{142}Gd, the rotation occurs around the longest axis owing to the distribution of neutron holes. In contrast, ^{89}Y (with $Z = 39$ and $N = 50$) exhibits a highly favorable rotation around the longest axis, characterized by a higher negative γ value of around -90°, due to the distribution of proton holes ($\pi((fp)^{-4}(g_{9/2})^3)$).

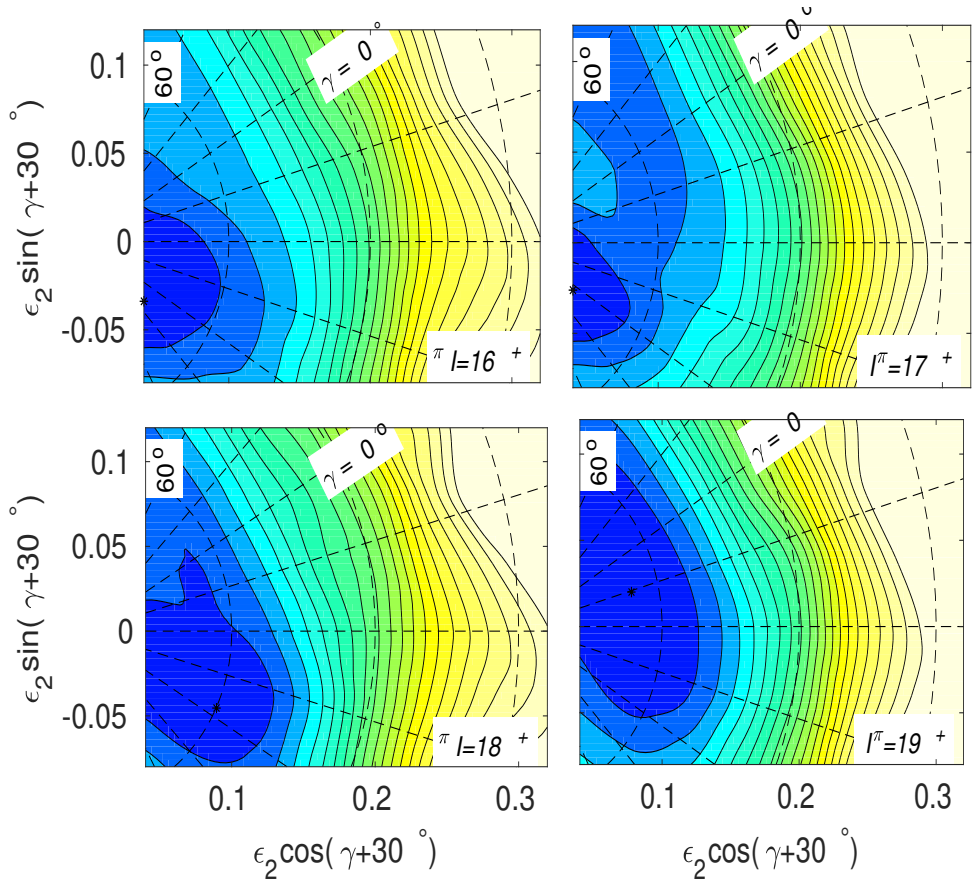

Figure 1.13 Calculated total energy surfaces plots for positive parity spin of 16$\hbar$, 17$\hbar$, 18 $\hbar$ and 19$\hbar$ for general scan in ^{90}Nb. The contour line separation is 0.25 MeV.

1.6 ^{90}Nb

A PES plot was drawn for a general scan run with positive parity configurations: For lower spin, the contour minimum mostly shows a non-collective prolate shape γ -120 ° (see

Fig.1.13). The ε_2 is very low, and it is quite expected for a near spherical nucleus. At $I \sim 18\hbar$ the shape is dominated by $\gamma \sim$ -60° whereas at $I \sim 18\hbar$ the minimum moves over to $\gamma \sim 15°$. This concludes that any energetically favorable configuration in ^{90}Nb should be stabilized within the observed energy minima. It is quite obvious nucleus should be more aligned towards shell model excitations. The major contribution to the high-spin states comes from the configuration with proton excitation across Z = 38 subshells.

1.7 ^{90}Zr

It is to be noted that ^{90}Zr is a semi-magic nucleus. As a result, the nucleus would prefer to attain extra stability compared to its nearest neighboring isotopes. Owing to this extra stability, it is obvious to pose the question of whether it will be energetically favorable to possess rotation around the longest principal axis even at high-spin states.

Two negative parity bands 2 and 3 [8] (shown in panel (b) of Fig. 1.9) are observed experimentally which are characterised by intra-band dipole transitions. In Fig. 1.14, the calculated energies for the band 2 and band 3 configurations are compared with those of the experimentally observed bands. The ground state band is compared with the positive parity [2;8] configurations. However, it is to be remembered that CNS calculations are pairing-independent. Hence, ground-state bands of any magic or semi-magic nucleus should be cautiously compared to the low-lying configurations. At the same time, the comparison between the ground state band and [2;8] shown in panel (c) of Fig. 1.14 shows a decreasing trend with an increase in spin. This is in accordance with the decrease in the pairing probability of nucleons with the increase in spin states. Therefore, the given configuration can be a good estimation for the ground state band in the nucleus. It is to be mentioned that we have compared the observed even spin states in the ground state band with those in the configuration [2;8]. Nevertheless, the experimental excitation energy vs spin (see panel(a) in Fig. 1.14) shows a probable band crossing around I = 8

$\hbar$. But, pairing the independent CNS model would not be a good choice for this comparison.

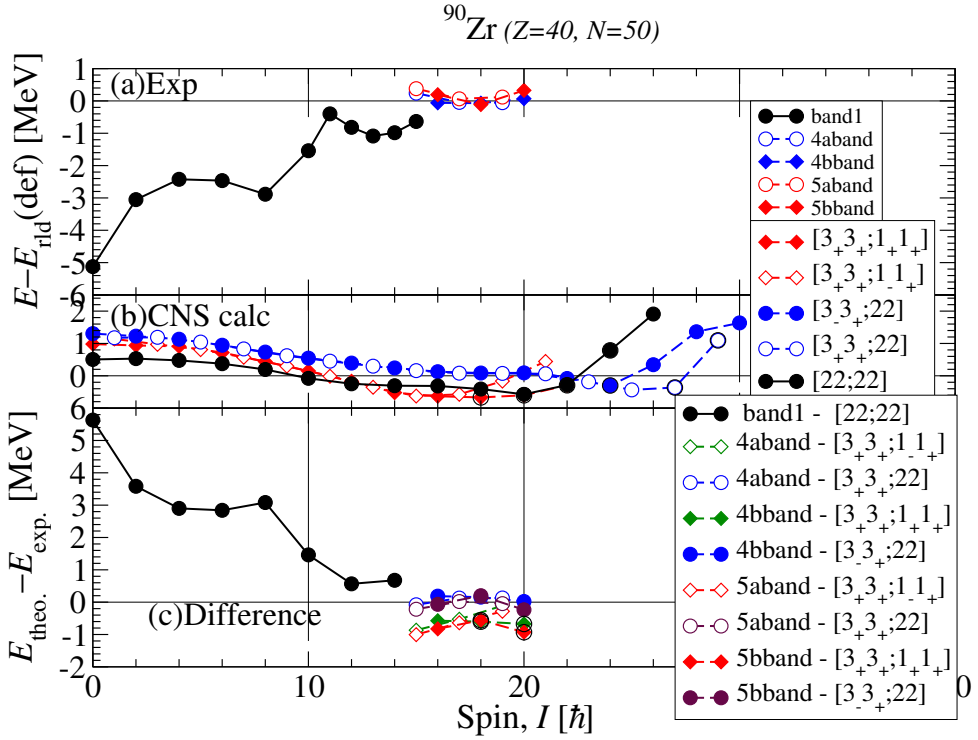

Figure 1.14 Excitation energies relative to rotating-liquid drop energy, for observed (upper panel) and calculated (lower panel) valence-space states for ^{90}Zr. Difference between the observed and calculated results have been shown in the third panel.

The even and odd spin states of band 4 have been compared with two configurations [33;11] and [33;22]. It is seen that configuration [33;22] agrees perfectly as the difference graph remains at a constant value near zero. Also, for configuration [33;11] calculated excitation energy is non-zero but stays at a constant negative value around -1 MeV. Therefore, the band 4 can be explained either by contribution from [33;11] $\pi((fp)^{-3}(g_{9/2})^3 \otimes \nu(g_{9/2})^{-1}(gd)^1)$ or [33;22] $\pi((fp)^{-3}(g_{9/2})^3 \otimes \nu(g_{9/2})^{-2}(gd)^2)$. Similarly, band 5 also agrees well with configurations [33;11] and [33;22] (see Fig. 1.14). So either bands 4 or 5 can be assigned with these two configurations. It was observed that the nucleus is stabilized with non-collective oblate shapes at different axial deformations.

This concludes that any energetically favorable configuration in ^{90}Zr should be stabilized within the observed energy minima. The energy contours for [33;11] configuration are shown in Fig. 1.15. For lower spin states of up to $16\hbar$, the shape is stabilized with a γ value of approximately 45° and ε_2 value of around 0.1, indicating rotation about the shortest principal axis. However, for higher spin states up to $I \sim 20\hbar$, the shape collapses to non-collective oblate. The proposed configurations using the CNS model agree well with the configurations predicted by the shell model [8].

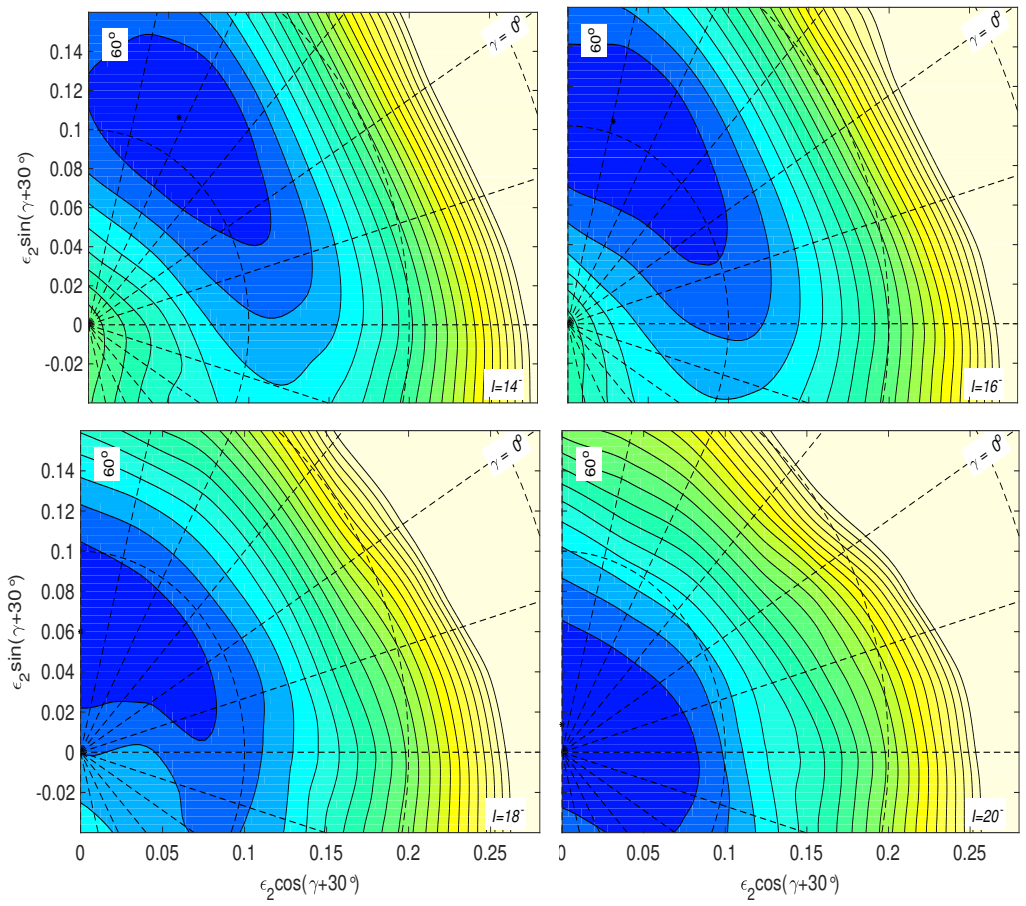

Figure 1.15 Calculated total energy surfaces plots for positive parity spin of $14\hbar$, $16\hbar$, $18\hbar$ and $20\hbar$ for [33;11] $\pi((fp)^{-3}g^{3}_{9/2})) \otimes \nu(g^{-1}_{9/2}(gd)^{1})$ in ^{90}Zr. The contour line separation is 0.25 MeV.

1.8 ^{91}Zr

The nucleus of ^{91}Zr ($Z = 40$, $N = 51$) has one neutron particle. A PES plot is drawn for a general scan run with positive parity configurations: Upto spin 19.5$\hbar$, the contour minimum shows non-collective oblate shape with $\gamma \sim 60°$ (see Fig.1.16). The ε_2 varies from 0.1 to 0.15 as the spin increases. It is quite obvious nucleus should be more aligned towards shell model excitations. The major contribution to the high-spin states comes from the configuration with neutron excitation across $N = 50$ subshells.

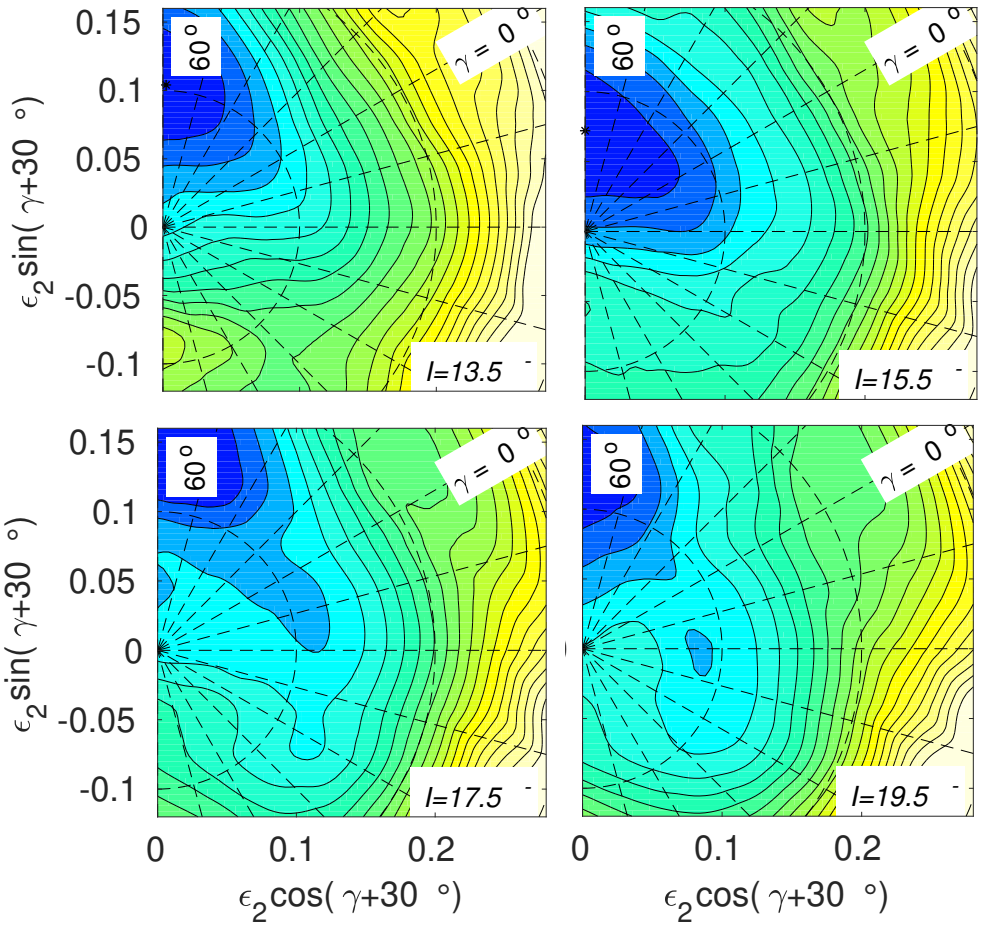

Figure 1.16 Calculated total energy surfaces plots for positive parity spin of 13.5$\hbar$, 15.5$\hbar$, 17.5$\hbar$ and 19.5$\hbar$ for general scan in ^{91}Zr. The contour line separation is 0.25 MeV

In conclusion, we can say that, in this mass region, both protons and neutrons occupy unique-parity $g_{9/2}$ orbitals. The protons filling up low-Ω $g_{9/2}$ orbitals favor prolate shapes (in case of ^{90}Nb) whereas oblate shapes are favored due to occupation of neutrons in medium-high-Ω $g_{9/2}$ orbitals (in case of ^{91}Zr).

The thesis mainly focuses on the results of the spectroscopic investigations of various nuclear shapes of $N = 51$ ^{92}Nb and $N = 52$ ^{93}Nb nuclei populated through the fusion-evaporation reaction ^{80}Se(^{18}O, p5n/p4n)^{92}Nb/^{93}Nb at a beam energy of 99 MeV.

1.9 Outline of the Thesis

The present thesis comprises seven chapters :

Chapter 1: Introduction: A brief introduction on the evolution of shapes, lifetime and isomers in nuclei has been presented. The survey of literature discussed extensively based on various experimental observations in $A \approx 90$ and their similarities with other mass regions are discussed.

Chapter 2: Experimental Techniques and Analysis Methods: Chapter 2 summarizes the details of the experimental instrumentation which have been used to populate the desired nuclei and on-line/off-line methodologies to study various properties of the same. The γ spectroscopy studies were performed with Indian National Gamma Array (INGA) spectrometer. High-spin states in nuclei were populated through fusion-evaporation reactions. Extensive level schemes of the nuclei under study have been analyzed with γ-γ matrices and γ-γ-γ cubes. Spin-parity of the excited states has been ascertained through angular distribution ratio and polarization measurements.

Chapter 3: Nuclear Models: The chapter briefly summarized nuclear models such as the liquid drop model, spherical and deformed shell model, the collective behavior of nuclear motion, cranking model and nuclear rotation for understanding nuclear structure. Finally, an elaborate discussion on cranked Nilsson Strutinsky (CNS) model.

Chapter 4: First lifetime measurement of the 9^- isomer in ^{92}Nb: The isomeric state at 9^- level was observed for the first time. In addition, the isomeric state at 11^- which was reported almost fifty years ago was remeasured and an excellent explanation of the state could be provided within the framework of the shell model calculations. The theoretical results for 9^- could not agree well with the experimental ones, and that may be due to excessive mixing.

Chapter 5: Core-excited states leading to the high-spin band structure in ^{93}Nb nucleus : The previously known level structure in ^{93}Nb has been rearranged owing to the observation of several high-energy γ transitions decaying from single-particle excited states to the aligned or anti-aligned states in the ground state band. Such transitions have presented a unique example of neutron and proton core-excited configurations. The level scheme was further updated with the addition of a few new transitions. The dipole band based on enhanced $M1$ transitions was verified and re-investigated through the life-time measurement of the corresponding levels using DSAM. Lifetimes were also measured for some of the $E2$ transitions in the ground state band. Extensive calculations were performed in the framework of CNS to show that the dipole band evolves with triaxial shape which is contrary to the earlier prediction of collective oblate shape.

Chapter 6: Rotation of ^{92}Nb nucleus about intermediate principal axes : The chapter discusses the spectroscopic study of ^{92}Nb using INGA. The nucleus is also studied within the framework of CNS model. Lifetime measurement in ^{92}Nb using DSAM.

Chapter 7: Conclusions and Future perspectives : The chapter summarizes the overall findings and observations as well as discusses future scopes in the context of the present thesis.

Appendix : The energy of transitions, intensities of the transitions, angular distribution ratio, spin-parity and energies of the levels, multipolarities and asymmetry ratio for the above mentioned three nuclei are given in tabular forms.